Article

Enhancement of Schottky Junction Silicon Solar Cell with CdSe/ZnS Quantum Dots Decorated Metal Nanostructures

Ha Trang Nguyen [1], Thanh Thao Tran [1], Vishwa Bhatt [1], Manjeet Kumar [1], Jinwon Song [2],* and Ju-Hyung Yun [1],*

1   Department of Electrical Engineering, Incheon National University, Incheon 406772, Korea; hatrangnguyen26@gmail.com (H.T.N.); thanhthao.apc@gmail.com (T.T.T.); vishwabhatt02.vb@gmail.com (V.B.); manuhp1@gmail.com (M.K.)
2   FINE LAB Co., Ltd., Daejeon 306230, Korea
*   Correspondence: jwsong@finelab.biz (J.S.); juhyungyun@inu.ac.kr (J.-H.Y.); Tel.: +82-42-931-9007 (J.S.); +82-32-835-8435 (J.-H.Y.); Fax: +82-42-931-9007 (J.S.); +82-32-835-0773 (J.-H.Y.)

Abstract: Recently, in the solar energy society, several key technologies have been reported to meet a grid parity, such as cost-efficient materials, simple processes, and designs. Among them, the assistive plasmonic of metal nanoparticles (MNPs) integrating with the downshifting on luminescent materials attracts much attention. Hereby, Si-based Schottky junction solar cells are fabricated and examined to enhance the performance. CdSe/ZnS quantum dots (QDs) with different gold nanoparticles (Au NPs) sizes were incorporated on a Si light absorbing layer. Due to the light scattering effect from plasmonic resonance, the sole Au NPs layer results in the overall enhancement of Si solar cell's efficiency in the visible spectrum. However, the back-scattering and high reflectance of Au NPs lead to efficiency loss in the UV region. Therefore, the QDs layer acting as a luminescent downshifter is deployed for further efficiency enhancement. The QDs layer absorbs high-energy photons and re-emits lower energy photons in 528 nm of wavelength. Such a downshift layer can enhance the overall efficiency of Si solar cells due to poor intrinsic spectral response in the UV region. The optical properties of Au NPs and CdSe QDs, along with the electrical properties of solar cells in combination with Au/QD layers, are studied in depth. Moreover, the influence of Au NPs size on the solar cell performance has been investigated. Upon decreasing the diameters of Au NPs, the blueshift of absorbance has been observed, cooperating with QDs, which leads to the improvement of the quantum efficiency in the broadband of the solar spectrum.

Keywords: plasmonic effect; downshifting; Schottky junction; Si-solar cell; Au NPs; CdSe/ZnS QDs

1. Introduction

Schottky junction solar cells have always been one of the most potential candidates for light energy conversion technology. Due to an uncomplicated and economical fabrication process, such as the direct deposition of a thin metal layer on a polycrystalline semiconductor wafer, the Schottky barrier has received high consideration from science society [1–3]. Unfortunately, this benefit concurrently turns into a drawback since the thickness of the thin metal layer will negatively impact the light absorption of the semiconductor [4]. Thanks to intense research efforts, several methods are issued to improve this matter [5–7]. Among them, plasmonic nano-antenna, such as metal nanostructures (MNS), are proposed as light harvesting for enhancing the overall performance of photonic devices [8–10]. The optical field strengthening from the localized surface plasmon resonance (LSPR) existing on the MNS could increase the photon absorbance into nearby materials. Besides, the solar spectra region of the surface plasmon resonance wavelength (λ_{SPR}) is strongly dependent on the size, shape, and concentration of MNS. Particularly, metal nanoparticles (MNPs) become very attractive due to their flexibility, straightforward synthetic, and high-uniform contribution [11,12]. Small sizes of MNPs (below 50 nm) are supposed to induce the intensive near-field localization; then, generate the light scattering in the board area of solar

spectra [13,14]. However, plasmon assistance of MNPs on the semiconductor wafer leads to the external quantum efficiency (EQE) loss in the UV and near UV region that has already been testified [15–18]. Additionally, quantum dots (QDs) luminescent layers are applied as the other approach to enhance solar cell efficiency. These layers absorb photons in the UV and near UV spectrum, then convert them into photons in the visible region to accumulate more incident photons [19–21]. Moreover, the properties of QDs, such as downshifting and anti-reflective, which facilitate the EQE enhancement of solar cells in the UV region, are demonstrated by research articles [22–24].

In this study, both plasmonic and luminescent materials are employed for enhancing the performance of silicon-based Schottky solar cells. CdSe/ZnS core/shell QDs and controlled sizes of gold nanoparticles (Au NPs) have been deployed to investigate the effect of hybrid structure on optoelectrical properties of the solar cell. This integration results in elevated EQE for the entire solar spectrum, averagely of 10%. The increase in the solar cell parameters, including the short circuit current (J_{SC}), the fill factor (FF), and the efficiency enhancement (η), are achieved of 20%, 8%, and 28%, respectively.

2. Materials and Methods

Reagents. CdSe/ZnS QDs were supplied from the FINE lab. Tetrachloroauric acid trihydrate ($HAuCl_4 \cdot _3H_2O$, 99.9+%), Oleylamine, and Sodium Hydroxide (NaOH) were acquired from Sigma Aldrich. Octanethiol, cyclohexane, and ethanol were provided from EMD Chemicals. Deionized water (Millipore Milli-Q grade) was handled in all experiments.

Synthesis of Au NPs-oil soluble. Au NPs with various sizes were synthesized by the standard chemical reduction of $HAuCl_4$, varying the volume of oleylamine [25]. Briefly, 3 mL of 1 wt.% $HAuCl_4$ was added to 70 mL DI water and then heated to boiling point. A quantity of 0.75 mL oleylamine was quickly added to the boiling solution under vigorous stirring for 2 h and allowed to cool to room temperature. For transferring the solution from water-soluble to oil-soluble, 30 mL cyclohexane was added to the above solution and stirred until the solution changed to ruby red color. To control the pH condition at the ideal value, 1.5 mL of 2 M NaOH was injected quickly into the mixture and stirred for 30 min. The solution was kept undisturbed at room temperature until it separated into two layers. The upper layer, including Au NPs, was allowed to precipitate by adding EtOH and purified by cyclohexane and EtOH once, then dispersed in 60 mL cyclohexane. For diverse Au NPs sizes, the volume of oleylamine was varied at 0.75, 1.0 mL, and 1.25 mL (corresponding to 3×10^{-2}, 4×10^{-2}, and 6×10^{-2} M, respectively) at a fixed $HAuCl_4$ concentration.

Fabrication of Si Schottky junction solar cells. For uncomplicated and reliable devices, the solar cells were fabricated on a 525 μm single polished n-type 1–10 Ω-cm Si wafer. For the back and front contact of the devices, 100 nm of titanium (Ti) and 5 nm of Au were deposited at 0.2 Å/s by thermal evaporation, respectively. Ti layer works as back contact, and Au film is responsible for the Schottky junction and oxidation barrier. Silver (Ag) front contact was deposited with a thickness of 100 nm using the grid pattern. For examining the effect of the Au/QDs layer on the devices, the synthesized Au NPs colloids and CdSe/ZnS QDs were coated layer-by-layer on the surface of solar cells by the spin coater as described in Figure 1.

Characterization. UV–Vis absorption spectrum was performed using an EMC-11-UV spectrophotometer (ranging from 300 nm to 1000 nm). Transmission electron microscopy (TEM) images were presented using TALOS F200X (S)TEM. PL spectra of samples were measured by a FluoTime300/MicroTime100 PicaQuant spectrometer (PicoQuant, 12489 Berlin, Germany) equipped with a dichroic filter and a 405 nm laser as the excitation source. For investigating the electrical properties of photovoltaic devices, the Keithley 4200-SCS system and IPCE PEC-S20 system were applied.
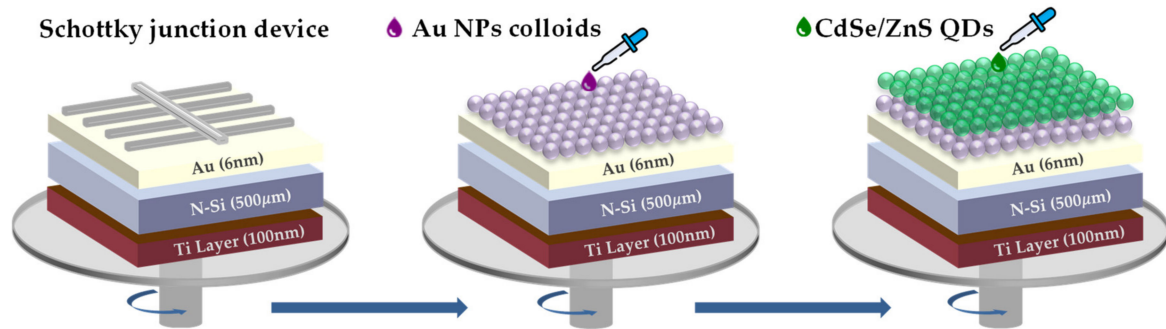
Figure 1. Schematic of device fabrication process.

3. Results and Discussions

An affordable and facile method for synthesizing different Au NPs is reported. The particles can be dissolved with both non-polar and polar solvents due to the powder form of the nanoparticles. TEM was carried out to investigate the size and morphology of the prepared Au NPs, and the results are reported in Figure 2a–c. Au NPs are mostly spherical and highly monodisperse; however, the smaller particle size shows the narrower size distribution. In detail, Au NPs 1 with the oleylamine concentration at 3×10^{-2} M has the largest average diameter of 24.8 ± 2.1 nm with a broad size distribution. Meanwhile, the highest concentration of oleylamine at 6×10^{-2} M produces Au NPs 3 with the smallest core particle size of 12.3 ± 0.6 nm. Additionally, the normalized absorption spectra of Au NPs (Figure 3a) with the plasmon absorption peaks of 524 nm, 523 nm, and 521 nm, in accordance with the Au NPs 1, Au NPs 2, and Au NPs 3. With increasing oleylamine concentration, the slight blue shift of Au NPs plasmon peak (from 524 nm to 521 nm) strongly confirms the particle size decrease. Thus, the particle diameters can be inferred from the oleylamine concentration. In the formation of oleylamine capped Au NPs complex, oleylamine plays a crucial role as both reducing and stabilizing agent [26]; as a result, the particle size and distribution can be tunned by the concentration of oleylamine.
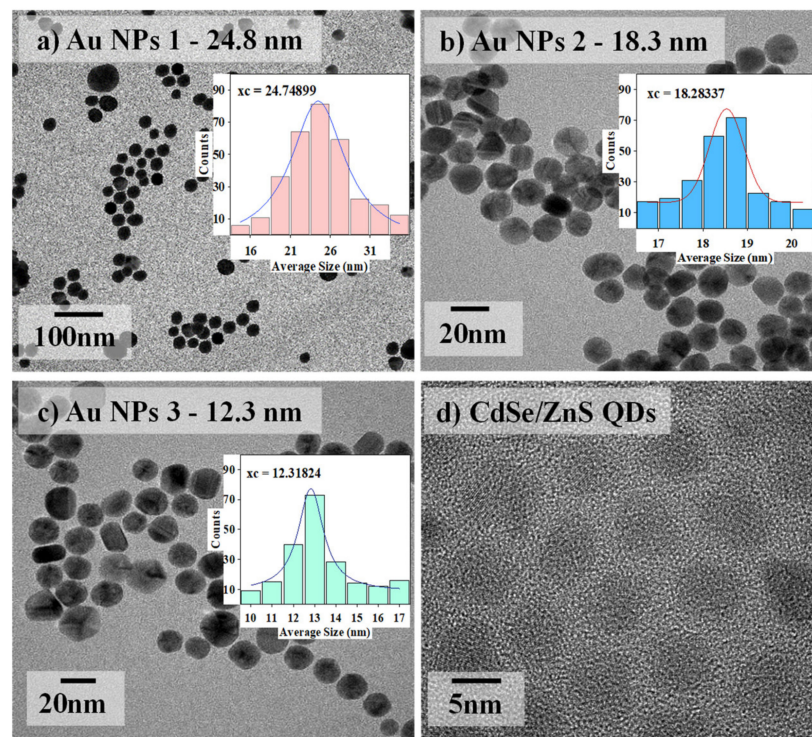

Figure 2. (**a**–**c**) TEM images of Au NPs. The insert shows the particle size distribution histogram of Au NPs. (**d**) TEM images of CdSe/ZnS QDs-528 nm.

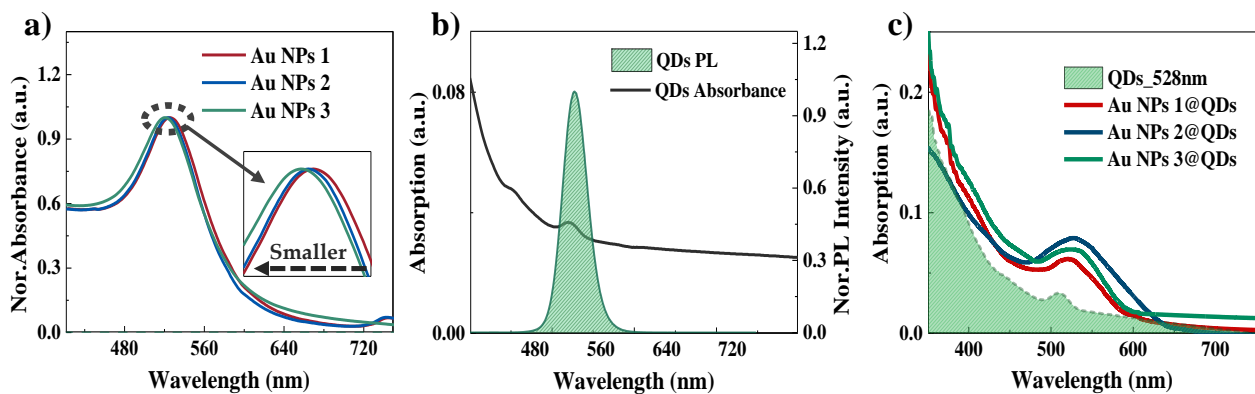**Figure 3.** (**a**) Normalized absorption spectra of Au NPs. (**b**) Absorption and emission spectra of CdSe/ZnS QDs. (**c**) Absorption spectra of QDs-528 nm individually and QDs-Au NPs conjugates.

In term of QDs, the green CdSe/ZnS core/shell QDs was employed. TEM image in Figure 2d indicates the narrow size distribution of QDs with an average diameter of ~3.6 nm. The absorption spectra and the PL emission spectra of QDs with the wavelength at 528 nm are presented in Figure 3b. The full width at half maximum (FWHM) is smaller than 35 nm. The quantum yield (QY) is about 85%, indicating high efficiency. The absorbance peak of QDs located at the wavelength of 508 nm, corresponding to the energy bandgap of 2.180 eV [27]. In the solar radiation spectrum, photons around 520 nm have the highest irradiance energy intensity that is useful for Silicon-based solar cells [28,29]. Compared to other CdSe QDs, the green one has a greater band gap, leading to a lower recombination rate in solar cells. Thus, CdSe/ZnS (green) is an potential candidate for enhancing PV performance [30,31].

To investigate the dependence of the LSPR effect on Au NPs and QDs, the absorption spectra of bare QDs and different Au NPs layers are measured, as shown in Figure 3c. With the addition of Au NPs, the overall absorbance intensity has increased. The SPR peaks and the accompanied FHWM are also obtained. The spectra peaks are located at 527 nm, 526 nm, and 523 nm. Correspondingly, the FWHM values are 68 nm, 80 nm, and 43 nm for Au NPs 1, Au NPs 2, and Au NPs 3. The lowest FHWM of Au NPs 3 indicates highly monodisperse particles. Besides, the variation in the absorbance intensity can be attributed to the surface coverage of the particles on thin film. It was reported that the spin coating Au NPs (<20 nm) gave the superior uniform shape and concentration on both glass and silicon substrates.

To understand the effect of Au/QD layer on PV performance, thin layers of Au NPs 2 (with a diameter of 18.3 nm) and CdSe QDs are adopted on the front side of the Schottky-based solar cell. Figure 4a displays the current density-voltage (J-V) characteristics of the devices under light illuminating conditions. Overall, the performance of solar cells has enhanced clearly after coating Au/QDs layer. After coating Au NPs layer, the considerable increase in J_{SC} from 14.86 mA/cm^2 to 17.07 mA/cm^2 and the slight growth in V_{OC} from 0.36 V to 0.37 V are observed. These improvements can be attributed to the enhanced IPCE (by 11%) in the wavelength segment ranging from 600 nm to 850 nm, presented in Figure 4b. This IPCE increase is assigned to the magnified light scattering effect [8–10]. However, the sole Au integrated solar cell reduces IPCE for photons possessing energy less than 2 eV, resulting from the back-scattering effect associated with Au NPs [15–18]. Meanwhile, the integration of cells with Au/QD layer further intensifies the J_{SC}, from 14.86 mA/cm^2 to 19.56 mA/cm^2, which is strongly suggested by the elevated IPCE value for broad spectrum. The hybrid Au/QDs structure overcomes the limit of sole embedded-Au NPs by the downshifting effect of QDs. The embedded hybrid structure-based solar cell provides an overall improved IPCE of 15% compared to bare Si-based solar cells.
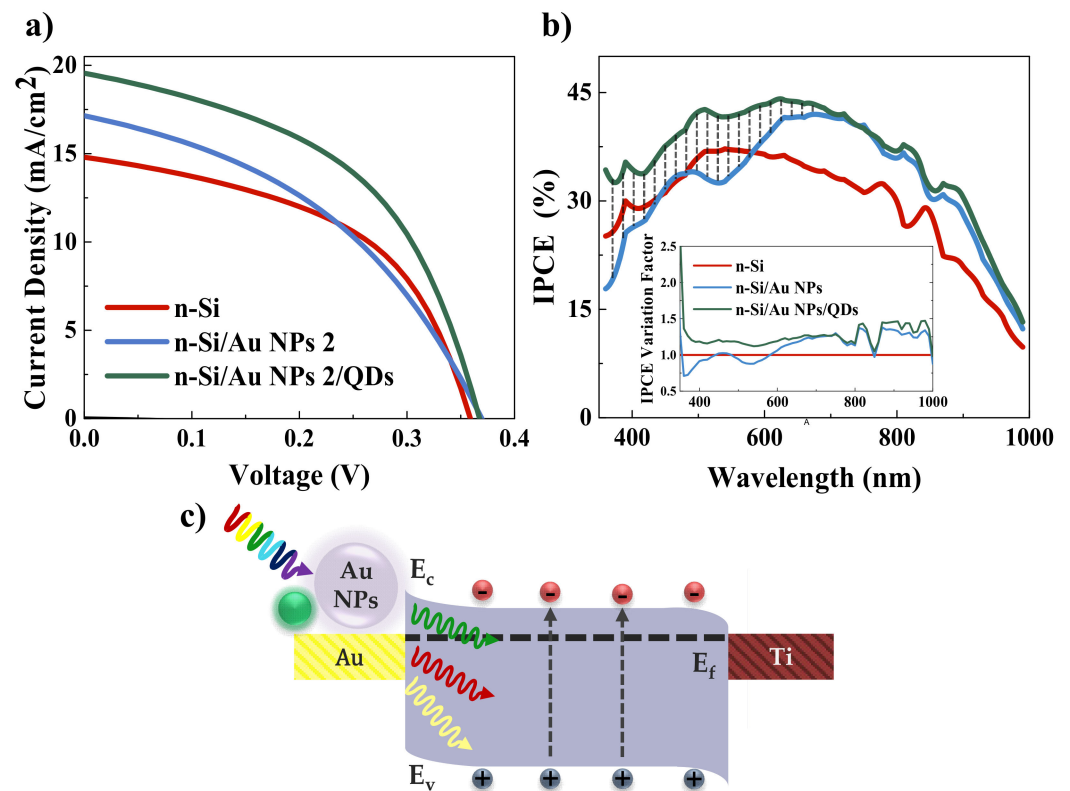
Figure 4. (**a**) Current density versus voltage curves. (**b**) Incident photon to current conversion efficiency (IPCE) spectra of all devices. (**c**) Energy band diagram at the equilibrium condition.

The photogeneration and separation process in the solar cell are studied by the proposed energy band diagram, as shown in Figure 4c. The work function of heavily doped n-type silicon with the resistivity of 1–10 Ωcm is reported as Φ_{Si} = 4.58 eV, and the bandgap is about 1.11 eV [32,33]. The work function of Au and Ti (Φ_{Au} & Φ_{Ti}) are 5.1 eV and 3.84 eV, respectively [34]. The higher work function of Au compared to n-Si results in the formation of built-in potential at the Au/n-Si interface. This built-in potential imposes the potential barrier height to the free electrons inside n-Si that leads to the formation of the Schottky junction. In addition, Φ_{Ti} is smaller than Φ_{Si} so that the Ohmic contact forms between Ti and n-Si. Under the light illuminating conditions, the -hole (e-h) pairs are generated by the photon absorption process. This includes two simultaneously interacting light procedures of Si, including direct light-source absorption and QDs induced light emission. The formed electric field as Schottky interface immediately separates the photo generated e^-/h^+ pairs. The separated carriers are swept away from the Au/Si junction under the drift mechanism to selective contact (electron to Ti and hole to Au); therefore, the photo-induced power is delivered to the external circuit. The enhanced performance of solar cells attributes to the synergetic effects, consisting of plasmonic effect and QDs downshifting.

To optimize the impact of Au NPs incorporated with QDs on the devices, three different sizes of prepared Au NPs were employed. The variation of photovoltaic parameters including J_{SC}, V_{OC}, FF, and η is described in Figure 5. It is observed patently that the smaller Au NPs diameter induced more enhancement in cell performance. In general, Au NPs 3 with the smallest size of 13.2 nm has the greatest effect on the Si-based Schottky solar cell performance. Specifically, FF and η increased up to 10% and 28%, respectively. The series (R_S) and shunt resistance (R_{SH}) are extracted from the dark J-V profile of the devices, presented by Figure 5c. After coating Au/QDs, the R_S increased from 1.001 Ω to 1.766 Ω, and the R_{SH} decreased from 595 Ω to 548 Ω. The observed resistance variation is negligible; therefore, the improved solar cell performance was primarily governed by the optical effect of Au/QDs hybrid structures. The solar cell parameters with Au NPs 3 and QDs are mentioned thoroughly in Table 1. As discussed, Au NPs 3 implies the most monodisperse

spherical particles and the highest surface coverage on the substrate among three particle sizes, thus contributing significantly to enhancing solar cell performance [35,36].
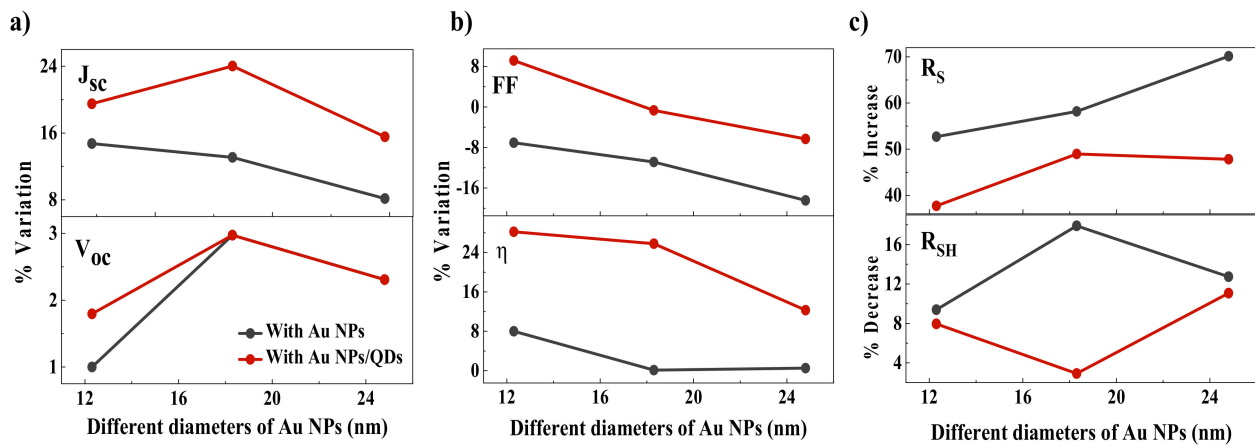

Figure 5. Variation of photovoltaic characteristics extracted for all devices with different diameters of Au NPs (**a**) J_{SC} and V_{OC}. (**b**) Fill factor and Efficiency. (**c**) Series resistance and Shunt resistance.

Table 1. J–V characteristics of reference cell, Au NPs 1 cell, and Au NPs 1/QDs composite cell measured under the artificial light.

Device	V_{oc} (V)	J_{sc} (mA/cm^2)	FF (%)	RS (Ω)	RSH (Ω)	η (%)
n-Si	0.383	15.535	42.493	1.101	595.854	2.528
n-Si/Au NPs	0.380	18.220	39.689	2.326	539.865	2.747
n-Si/Au NPs/QDs	0.387	19.299	46.791	1.766	548.481	3.495

By measuring the electrical properties of devices, the influence of Au NPs and QDs in the cell's performance is clarified. The increase in the broadband region between 600 nm and 850 nm is considered to be attributed to the plasmonic effect of Au NPs [15,17]. As mentioned, the significant absorbance in the UV range and the high photon emission intensity at 528 nm are the well-assist factors for significantly increasing light absorption in the Si layer, which contributes to the J_{SC} enhancement [23]. Besides, QDs is also recognized as its anti-reflective property so that the photon absorption can be increased, which induce the improvement in the carrier concentration and the photoconductivity in the solar cell [37–40].

4. Conclusions

In summary, we introduced a flexible methodology for enhancing solar cell performance. By depositing Au NPs and CdSe/ZnS QDs layer-by-layer in Si-based Schottky solar cells, a considerable increase in cell performance is observed. Besides, the effect of different Au NPs diameters is explored. Without coating QDs layers on the cells, the smallest diameter of controlled Au NPs sizes has given the highest efficiency enhancement, up to 8%, corresponding with the photocurrent heightening of 14%. Moreover, the efficiency depicts remarkable improvement by incorporating Au NPs with CdSe/ZnS layer on the cells. In detail, the best cell's performance at the smallest Au NPs attains 28% efficiency enhancement. This can be explained by the downshifting of incident photons and the anti-reflectance property of QDs. This facile method can be well-incorporated with Si-based Schottky solar cells and other types of devices, such as dye-sensitized (DSSCs) and organic solar cells.

References

1. Chowdhury, K.; Mandal, R. Advancement of Schottky Barrier Solar Cells: A Review. *ICID* **2020**, *2*, 93–98.
2. You, A.; Be, M.A.Y.; In, I. The physics and chemistry of the Schottky barrier height. *Appl. Phys. Rev.* **2018**, *1*, 011304.
3. Kong, X.; Zhang, L.; Liu, B.; Gao, H.; Zhang, Y.; Yan, H.; Song, X. Graphene/Si Schottky solar cells: A review of recent advances and prospects. *RSC Adv.* **2019**, *9*, 863–877. [CrossRef]
4. Dasgupta, K.; Chowdhury, K.; Mondal, A.; Ray, S.; Gangopadhyay, U. Advancement and Challenges for Schottkey Barrier MIS/SIS Solar Cells: A Review. *Trans. Indian Natl. Acad. Eng.* **2021**, 1–16. [CrossRef]
5. Zhang, C.; Guney, D.O.; Pearce, J.M. Plasmonic enhancement of amorphous silicon solar photovoltaic cells with hexagonal silver arrays made with nanosphere lithography. *Mater. Res. Express* **2016**, *3*, 105034. [CrossRef]
6. Godfrey, R.B.; Green, M.A. 655 mV open-circuit voltage, 17.6% efficient silicon MIS solar cells. *Appl. Phys. Lett.* **1979**, *34*, 790–793. [CrossRef]
7. Atwater, H.A.; Polman, A. Plasmonics for improved photovoltaic devices. *Nat. Mater.* **2010**, *9*, 205–213. [CrossRef]
8. Zhou, N.; López-Puente, V.; Wang, Q.; Polavarapu, L.; Pastoriza-Santos, I.; Xu, Q.H. Plasmon-enhanced light harvesting: Applications in enhanced photocatalysis, photodynamic therapy and photovoltaics. *RSC Adv.* **2015**, *5*, 29076–29097. [CrossRef]
9. Aubry, A.; Lei, D.Y.; Fernández-Domínguez, A.I.; Sonnefraud, Y.; Maier, S.A.; Pendry, J.B. Plasmonic light-harvesting devices over the whole visible spectrum. *Nano Lett.* **2010**, *10*, 2574–2579. [CrossRef]
10. Naphade, R.A.; Tathavadekar, M.; Jog, J.P.; Agarkar, S.; Ogale, S. Plasmonic light harvesting of dye sensitized solar cells by Au-nanoparticle loaded TiO₂ nanofibers. *J. Mater. Chem. A* **2014**, *2*, 975–984. [CrossRef]
11. Bonatti, L.; Gil, G.; Giovannini, T.; Corni, S.; Cappelli, C. Plasmonic Resonances of Metal Nanoparticles: Atomistic vs. Continuum Approaches. *Front. Chem.* **2020**, *8*, 340. [CrossRef]
12. Shi, H.; Zhu, X.; Zhang, S.; Wen, G.; Zheng, M.; Duan, H. Plasmonic metal nanostructures with extremely small features: New effects, fabrication and applications. *Nanoscale Adv.* **2021**, *3*, 4349–4369. [CrossRef]
13. Liu, B.J.; Lin, K.Q.; Hu, S.; Wang, X.; Lei, Z.C.; Lin, H.X.; Ren, B. Extraction of absorption and scattering contribution of metallic nanoparticles toward rational synthesis and application. *Anal. Chem.* **2015**, *87*, 1058–1065. [CrossRef]
14. Van Dijk, M.A.; Tchebotareva, A.L.; Orrit, M.; Lippitz, M.; Berciaud, S.; Lasne, D.; Cognet, L.; Lounis, B. Absorption and scattering microscopy of single metal nanoparticles. *Phys. Chem. Chem. Phys.* **2006**, *8*, 3486–3495. [CrossRef]
15. Karber, E.; Katerski, A.; Acik, I.O.; Mikli, V.; Mere, A.; Sildos, I.; Krunks, M. Low-cost plasmonic solar cells prepared by chemical spray pyrolysis. *Beilstein J. Nanotechnol.* **2014**, *5*, 2398–2402. [CrossRef]
16. Van Dijk, L.; Van De Groep, J.; Veldhuizen, L.W.; Di Vece, M.; Polman, A.; Schropp, R.E.I. Plasmonic Scattering Back Reflector for Light Trapping in Flat Nano-Crystalline Silicon Solar Cells. *ACS Photonics* **2016**, *3*, 685–691. [CrossRef]
17. Ho, W.J.; Lee, Y.Y.; Su, S.Y. External quantum efficiency response of thin silicon solar cell based on plasmonic scattering of indium and silver nanoparticles. *Nanoscale Res. Lett.* **2014**, *9*, 1–8. [CrossRef]
18. Tong, C.; Yun, J.; Song, H.; Gan, Q.; Anderson, W.A. Plasmonic-enhanced Si Schottky barrier solar cells. *Sol. Energy Mater. Sol. Cells* **2014**, *120*, 591–595. [CrossRef]
19. Rezaee, G.; Mortazavi, S.Z.; Mirershadi, S.; Reyhani, A. Efficiency enhancement of CdSe quantum dots assisted Si-solar cell. *J. Mater. Sci. Mater. Electron.* **2018**, *29*, 500–508. [CrossRef]
20. Amiri, O.; Salavati-Niasari, M.; Bagheri, S.; Yousefi, A.T. Enhanced DSSCs efficiency via Cooperate co-absorbance (CdS QDs) and plasmonic core-shell nanoparticle (Ag@PVP). *Sci. Rep.* **2016**, *6*, 25227. [CrossRef]
21. Vinoth Pandi, D.; Muthukumarasamy, N.; Agilan, S.; Velauthapillai, D. CdSe quantum dots sensitized ZnO nanorods for solar cell application. *Mater. Lett.* **2018**, *223*, 227–230. [CrossRef]
22. Flores-Pacheco, A.; Álvarez-Ramos, M.E.; Ayón, A. Chapter Thirteen—Down-Shifting by Quantum Dots for Silicon Solar Cell Applications. In *Solar Cells and Light Management*; Enrichi, F., Righnini, G.C., Eds.; Elsevier: Amsterdam, The Netherlands, 2019; Volume 13, pp. 443–477.

23. Lopez-Delgado, R.; Zhou, Y.; Zazueta-Raynaud, A.; Zhao, H.; Pelayo, J.E.; Vomiero, A.; Álvarez-Ramos, M.E.; Rosei, F.; Ayon, A. Enhanced conversion efficiency in Si solar cells employing photoluminescent down-shifting CdSe/CdS core/shell quantum dots. *Sci. Rep.* **2017**, *7*, 14104.

24. Jeong, H.J.; Kim, Y.C.; Lee, S.K.; Jeong, Y.; Song, J.W.; Yun, J.H.; Jang, J.H. Ultrawide Spectral Response of CIGS Solar Cells Integrated with Luminescent Down-Shifting Quantum Dots. *ACS Appl. Mater. Interfaces* **2017**, *9*, 25404–25411. [CrossRef]

25. Mourdikoudis, S.; Liz-Marzán, L.M. Oleylamine in nanoparticle synthesis. *Chem. Mater.* **2013**, *25*, 1465–1476. [CrossRef]

26. Aslam, M.; Fu, L.; Su, M.; Vijayamohanan, K.; Dravid, V.P. Novel one-step synthesis of amine-stabilized aqueous colloidal gold nanoparticles. *J. Mater. Chem.* **2004**, *14*, 1795–1797. [CrossRef]

27. Cheng, C.; Yan, H. Bandgap of the core-shell CdSe/ZnS nanocrystal within the temperature range 300–373 K. *Phys. E Low-Dimens. Syst. Nanostruct.* **2009**, *41*, 828–832. [CrossRef]

28. Tanaka, Y.; Matsuo, K. Non-Thermal Effects of Near-Infrared Irradiation on Melanoma. In *Breaktroughs in Melanoma Research*; Intech Open: Rijeka, Croatia, 2011; Volume 29, pp. 597–628.

29. Meng, L.; Wu, X.G.; Ma, S.; Shi, L.; Zhang, M.; Wang, L.; Chen, Y.; Chen, Q.; Zhong, H. Improving the efficiency of silicon solar cells using in situ fabricated perovskite quantum dots as luminescence downshifting materials. *Nanophotonics* **2020**, *9*, 93–100. [CrossRef]

30. Baek, S.W.; Shim, J.H.; Seung, H.M.; Lee, G.S.; Hong, J.P.; Lee, K.S.; Park, J.G. Effect of core quantum-dot size on power-conversion-efficiency for silicon solar-cells implementing energy-down-shift using CdSe/ZnS core/shell quantum dots. *Nanoscale* **2014**, *6*, 12524–12531. [CrossRef]

31. Tavakoli, M.M.; Prochowicz, D.; Yadav, P.; Tavakoli, R. Efficient Perovskite Solar Cells Based on CdSe/ZnS Quantum Dots Electron Transporting Layer with Superior UV Stability. *Phys. Status Solidi Rapid Res. Lett.* **2020**, *14*, 2000062. [CrossRef]

32. Novikov, A. Experimental measurement of work function in doped silicon surfaces. *Solid-State Electron.* **2010**, *54*, 8–13. [CrossRef]

33. Aboelfotoh, M.O.; Cros, A.; Svensson, B.G.; Tu, K.N. Schottky-barrier behavior of copper and copper silicide on n-type and p-type silicon. *Phys. Rev. B* **1990**, *41*, 9819–9827. [CrossRef] [PubMed]

34. Kumar, B.; Kaushik, B.K.; Negi, Y.S. Perspectives and challenges for organic thin film transistors: Materials, devices, processes and applications. *J. Mater. Sci. Mater. Electron.* **2014**, *25*, 1–30. [CrossRef]

35. Ng, S.A.; Razak, K.A.; Aziz, A.A.; Cheong, K.Y. The effect of size and shape of gold nanoparticles on thin film properties. *J. Exp. Nanosci.* **2014**, *9*, 64–77. [CrossRef]

36. Livshits, P.; Inberg, A.; Shacham-Diamand, Y.; Malka, D.; Fleger, Y.; Zalevsky, Z. Precipitation of gold nanoparticles on insulating surfaces for metallic ultra-thin film electroless deposition assistance. *Appl. Surf. Sci.* **2012**, *258*, 7503–7506. [CrossRef]

37. Shao, W.; Lu, P.; Li, W.; Xu, J.; Xu, L.; Chen, K. Simulation and Experimental Study on Anti-reflection Characteristics of Nano-patterned Si Structures for Si Quantum Dot-Based Light-Emitting Devices. *Nanoscale Res. Lett.* **2016**, *11*, 1–7. [CrossRef] [PubMed]

38. Jeong, H.J.; Kim, Y.C.; Lee, S.K.; Yun, J.H.; Jang, J.H. Enhanced spectral response of CIGS solar cells with anti-reflective subwavelength structures and quantum dots. *Sol. Energy Mater. Sol. Cells* **2019**, *194*, 177–183. [CrossRef]

39. Krishnan, C.; Mercier, T.; Rahman, T.; Piana, G.; Brossard, M.; Yagafarov, T.; To, A.; Pollard, M.E.; Shaw, P.; Bagnall, D.M.; et al. Efficient light harvesting in hybrid quantum dot-interdigitated back contact solar cells: Via resonant energy transfer and luminescent downshifting. *Nanoscale* **2019**, *11*, 18837–18844. [CrossRef]

40. Farahani, F.A.; Poro, A.; Rezaee, M.; Sameni, M. Enhancement in power conversion efficiency of CdS quantum dot sensitized solar cells through a decrease in light reflection. *Opt. Mater.* **2020**, *108*, 110248. [CrossRef]